Crystal-field effects in amorphous DyX alloys (X=Al, Ga, Au) from ^{161}Dy Mössbauer-effect and bulk magnetic results

M. Maurer and J. M. Friedt
Centre De Recherches Nucleaires, 67037 Strasbourg Cedex, France
(Received 2 March 1984)

^{161}Dy Mössbauer spectroscopy and static and dynamic magnetic properties are investigated in a series of amorphous Dy alloys ($Dy_{80}Au_{20}$, $Dy_{80}Ga_{20}$, $Dy_{65}Al_{35}$) presenting different structural short-range orders. The bulk properties demonstrate the onset of an asperomagnetic order via a spin-glass-like transition. The temperature dependence of the hyperfine parameters and of their distribution below T_f are interpreted in the molecular-field approximation using a nonaxial quadratic crystal-field model. Satisfactory agreement between theory and experiment is obtained with the parameters B_2^0 and B_2^2 evaluated experimentally from electric-field-gradient results at S-state rare-earth atoms ($R=Eu^{2+}$, Gd^{3+}) in the corresponding $R_{1-x}X_x$ amorphous alloys. The consideration of the nonaxial quadratic crystal-field Hamiltonian is found to be necessary and sufficient in order to represent experiments in the considered amorphous Dy alloys.

I. INTRODUCTION

The magnetism of amorphous rare-earth (RE) alloys is usually described in terms of random magnetic anisotropy (RMA) effects, arising from competing exchange and crystalline electric field (CEF) interactions.[1] In amorphous media, contrary to crystalline materials, symmetry considerations cannot be invoked for selecting the relevant CEF terms B_l^m. On the basis of computer simulations, the truncation of the CEF Hamiltonian to the second-order terms (B_2^0,B_2^2) represents an acceptable approximation.[1] Indeed, a point-charge calculation of the CEF parameters establishes that the quadratic contribution to the overall CEF splitting exceeds by 1 order of magnitude the effect of higher-order terms.

Thus, with the magnetic exchange represented in the molecular-field ($H_{\rm mol}$) model, the single-ion electronic Hamiltonian is approximated as

$$\mathcal{H}=\mathcal{H}_{\rm CEF}+\mathcal{H}_M=B_2^0O_2^0+B_2^2O_2^2-g_J\mu_B\vec{J}\cdot\vec{H}_{\rm mol} \quad (1)$$

with the local CEF reference frame at random orientation at every RE site. O_2^0 and O_2^2 represent Stevens equivalent operators, g_J is the Landé factor, μ_B the Bohr magneton, and $\vec{J}$ is the total angular momentum vector. In the presence of magnetic exchange being dominantly ferromagnetic, the above model implies a random orientation between $\vec{J}$ and $\vec{H}_{\rm mol}$.

The quenching of the local angular momentum into random direction is consistently argued from computer simulations[1] and from the overall agreement of bulk data with Eq. (1). It is also consistent with the random orientation between the hyperfine field (H) and the electric-field-gradient (EFG) principal axis measured in magnetic S-state R (Eu, Gd) (R is the rare earth) amorphous alloys.[2]

For amorphous alloys including heavy RE elements (i.e., with large J value), bulk magnetic properties and specific-heat data are generally well represented using a RMA model restricted to the uniaxial CEF term ($B_2^2=0$).[1,3–5] However, the physical significance of these results should be considered with caution: For instance, the B_2^0 term is systematically deduced to be of negative sign whereas in an homogeneous series of amorphous RE alloys with constant structural short-range order one would expect a change in sign according to the sign of the Stevens coefficient α_J for the specific RE element. Phenomenologically, this approach is equivalent to a local easy axis on every RE site, which is oriented at random with respect to any macroscopic reference direction.

In light RE alloys, i.e., for small angular momentum J, the consideration of the nonaxial quadratic term (B_2^2) is required in order to represent the bulk magnetic results.[6,7] The most direct demonstration for the uniaxial RMA model has been based on ^{161}Dy Mössbauer-spectroscopy results.[1,8] Indeed, a narrow distribution of the EFG, along with a reduction with respect to the free-ion value, was claimed to demonstrate a strict angular correlation between the lattice and the $4f$ contributions to the EFG, i.e., by definition, the uniaxial RMA. This conclusion is revised critically in the present work on the basis of a detailed analysis of the distributions of hyperfine parameters and of their successful description using the nonaxial RMA Hamiltonian [Eq. (1)] in a series of amorphous dysprosium alloys. The quadratic CEF parameters are known in the considered alloys from the "lattice" EFG parameters measured in the corresponding Eu and Gd alloys, under the acceptable approximation that the structural short-range order is independent of the specific RE element.[9] This procedure provides a physical interpretation of the electronic Hamiltonian [Eq. (1)], in contrast with the common phenomenological application of the uniaxial approximation to bulk properties. The former demonstration for the uniaxial RMA from ^{161}Dy Mössbauer results is found oversimplified. From a microscopical point of view, the consideration of at least all the terms in Eq. (1) (i.e., B_2^2, B_2^0 in sign) is necessary (and sufficient) for representing the experimental ^{161}Dy hyper-

fine results.

The alloys selected for investigation ($Dy_{80}Au_{20}$, $Dy_{80}Ga_{20}$, $Dy_{65}Al_{35}$) display different local structures, extending from essentially axial symmetry in $Dy_{80}Au_{20}$ to distributed lower symmetry in $Dy_{65}Al_{35}$.[9] Hence, it is of interest to investigate how these structural differences may be reflected from the hyperfine data and the RMA parameters.

II. EXPERIMENTAL PROCEDURE

The amorphous alloys were prepared by melt spinning under purified argon gas.[9] The same ribbons were used in all experiments.

The dynamic susceptibility (χ_{ac}) was recorded at 3.5 kHz as a function of temperature using a lock-in amplifier. Several ribbons of each alloy were measured separately in order to check for homogeneity. Magnetization was determined by the extraction method, using a superconducting magnet. Static susceptibility (χ_{dc}) was measured with the help of a Faraday balance (Oxford Instruments), operating at a field of 8.45 kG and at a gradient of 100 G/cm.

^{161}Dy Mössbauer spectra were run with a $^{160}Gd^{162}DyF_3$ source kept at room temperature (minimum experimental linewidth of 4 mm/s). Either Xe-CO_2 or Ge detectors were employed, according to the activity of the source. Least-squares computer fitting for the distributed hyperfine parameters was achieved by summation of several 16-line magnetic subspectra; the component intensities correspond to the isotropic situation. Various polynomial distributions of the hyperfine field and of the quadrupole interaction were tested. A histogram fit was also used in order to check for consistency of the analytical distributions. In all cases, in the magnetically ordered phases satisfactory fits were obtained using a phenomenological probability for the hyperfine field distribution [i.e., $P(H)=P(H_{max}-n\Delta H)\propto(1-\frac{1}{10}n)^3$ for $0\leq n\leq 10$ and $P(H)=0$ elsewhere] and fitting H_{max} and ΔH.

III. EXPERIMENTAL RESULTS

A. Bulk magnetic properties

In all three $Dy_{1-x}X_x$ alloys (X=Au, Ga, Al) under consideration, the dynamic susceptibility (χ_{ac}) displays a sharp cusp at a temperature T_f (Fig. 1, Table I), similar to observations for spin-glass transitions. The static susceptibility (χ_{dc}) follows a Curie-Weiss law at high temperature, i.e., $T\geq 85$ K (Fig. 1). The paramagnetic moments (μ_p) are in agreement with the free-ion (FI) value for Dy^{3+}: $\mu_p^{FI}=10.64\mu_B/Dy^{3+}$ atom (Table I). The positive paramagnetic Curie temperatures Θ_p (Table I) indicate dominant ferromagnetic exchange interactions.

dc magnetization below T_f displays the behavior characteristic for ferromagnetism in the presence of random anisotropy, i.e., a large reduction of the spontaneous moments and an absence of saturation up to the largest available field (50 kOe) (Fig. 2). The temperature dependence of the magnetization $\sigma(H_a,T)$ measured in an applied field of 40 kOe demonstrates a nearly constant moment up to T_f and a subsequent progressive decrease (Fig. 3).

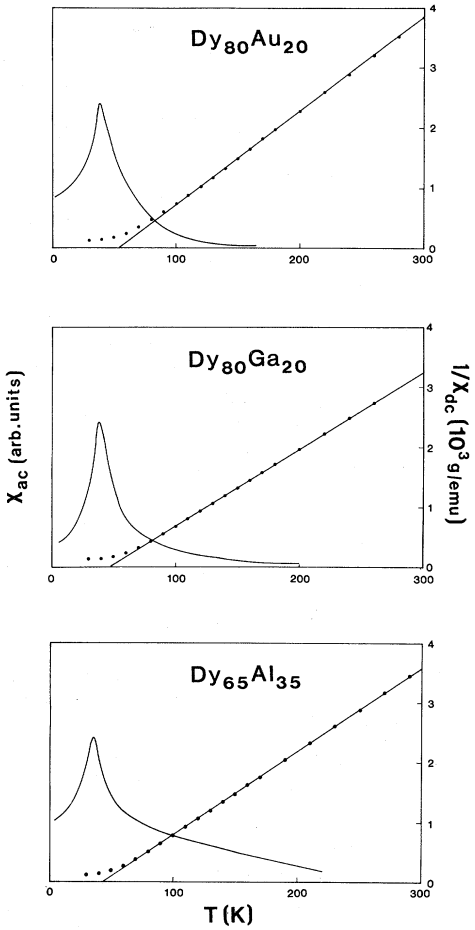

FIG. 1. Temperature dependences of the dynamic susceptibility (χ_{ac}) and of the inverse dc field susceptibility ($1/\chi_{dc}$) in the amorphous Dy-based alloys.

B. ^{161}Dy Mössbauer spectroscopy

The temperature dependence of the Mössbauer spectra reveals three distinct regimes in all the considered alloys: Below T_f, static magnetic hyperfine spectra are observed. They are comparable for all alloys (Figs. 4 and 5). Above

TABLE I. Bulk magnetic properties of amorphous $Dy_{1-x}X_x$ alloys. The T^* are scaled with the de Gennes factor from the Curie temperatures of the corresponding amorphous $Gd_{80}X_{20}$ alloys.

	$Dy_{80}Au_{20}$	$Dy_{80}Ga_{20}$	$Dy_{65}Al_{35}$
Θ_p (K)	54±1	48±1	44±1
μ_p (μ_B/Dy^{3+} at.)	10.4±0.2	10.7±0.2	10.1±0.2
T_f (K)	38±2	37±2	36±2
σ(4.2 K, 40 kG) (μ_B/Dy at.)	6.0±0.2	5.6±0.2	4.9±0.2
T^* (K)	67[a]	58[b]	65[b]

[a]Reference 10.
[b]Reference 11.

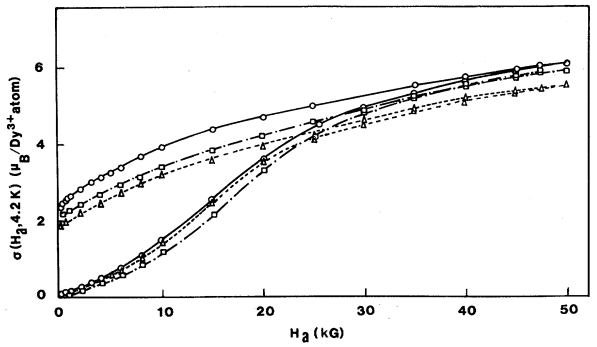

FIG. 2. Magnetization $\sigma(H_a, 4.2\ \mathrm{K})$ at 4.2 K versus the applied field H_a. ○, $Dy_{80}Au_{20}$; □, $Dy_{80}Ga_{20}$; △, $Dy_{65}Al_{35}$.

T_f, in an intermediate temperature range ($T_f \leq T < 2T_f$) smeared magnetic hyperfine spectra appear, whereas at still larger temperature ($T > 2T_f$) they collapse into a broad single resonance.

In the ordered phases, consistent fits are achieved in terms of a skewed distribution for the hyperfine field H (which is well represented by a cubic polynomial function) and a narrow distribution for the quadrupole coupling constant (Figs. 4–6, Table II). The poor precision of the deduced parameter distributions (Fig. 6) is readily realized from the limited resolution of ^{161}Dy Mössbauer spectroscopy since the minimum experimental width (4 mm/s) corresponds to a quadrupole coupling constant of 13 mm/s and a hyperfine field of 100 kOe. In particular, the shape of the distribution of EFG parameters cannot be analyzed with any precision; it should be noticed that the width of the distribution is comparable with the error on its measurement.

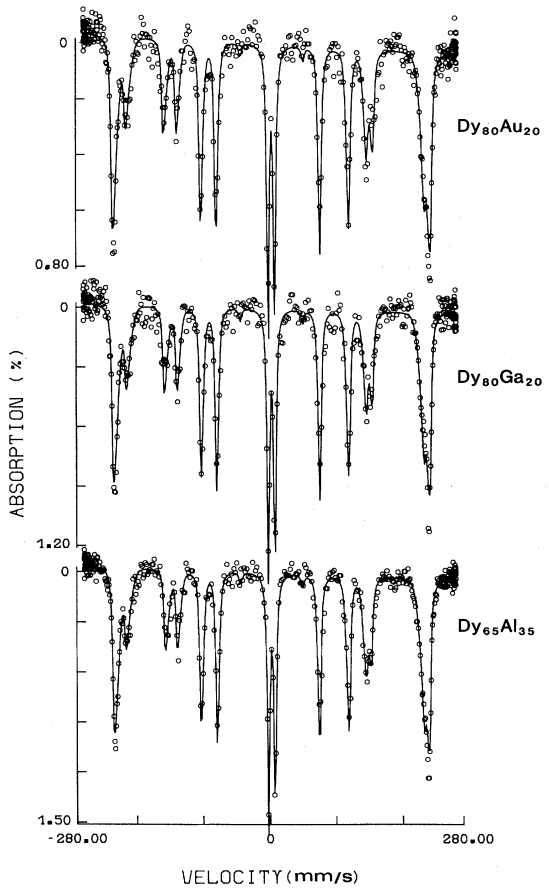

FIG. 4. ^{161}Dy Mössbauer spectra at $T = 4.2$ K in amorphous Dy-based alloys. The heavy lines represent best fits as discussed in the text

IV. DISCUSSION OF THE BULK MAGNETIC PROPERTIES

The whole of the static and dynamic susceptibility and magnetization results are typical for magnetism in the presence of random magnetic anisotropy. The homogeneous transition to an asperomagnetic state at T_f is consistently detected by ac susceptibility and Mössbauer spectroscopy.

A departure from a normal paramagnetic behavior is observed above T_f (up to $\sim 2T_f$) in terms of a large deviation of χ_{dc} from a Curie-Weiss law and of a slow decrease in magnetization above T_f (Figs. 1 and 3). This is assigned to magnetic short-range order in this temperature regime, similar to direct evidence from small-angle neutron scattering in comparable amorphous alloys.[12,13]

The combined singular bulk magnetic and hyperfine results above T_f are assigned to relaxation in an intermediate temperature range extending from T_f to about $2T_f$.[14] At still higher temperature, the Mössbauer line shape is assigned to single-ion paramagnetic relaxation effects.

The significant reduction of the magnetic ordering temperatures (T_f) in comparison to Θ_p (Table I) indicates frustration of magnetic interactions by random anisotropy effects. This conclusion is furthermore supported from a comparison of the experimental T_f's with the ones which are estimated in the absence of such frustration: Indeed, scaling the Curie temperatures of the corresponding ferromagnetic Gd compounds with the de Gennes factor $(g_J - 1)^2 J(J+1)$ provides pseudo-ordering temperatures (T^*, Table I) which significantly exceed T_f.

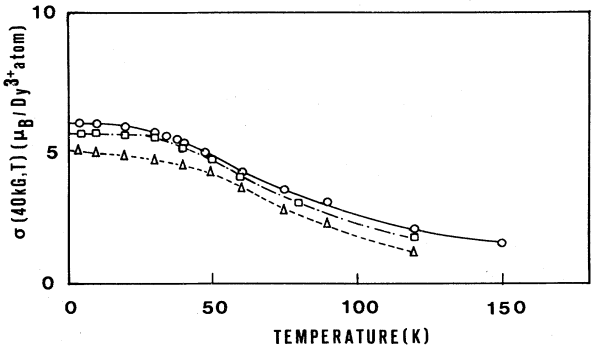

FIG. 3. Magnetization $\sigma(40\ \mathrm{kG}, T)$ in a constant applied field $H_a = 40$ kG versus temperature T. ○, $Dy_{80}Au_{20}$; □, $Dy_{80}Ga_{20}$; △, $Dy_{65}Al_{35}$.

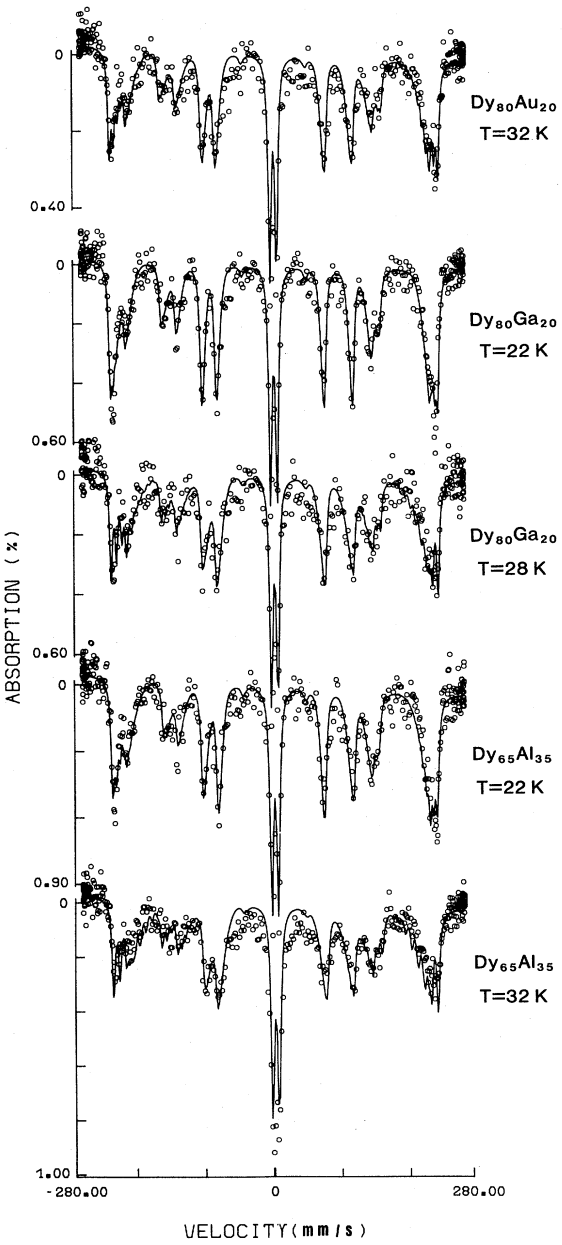

FIG. 5. ^{161}Dy Mössbauer spectra as a function of temperature below T_f in amorphous Dy alloys. The heavy lines represent best fits including both a skewed hyperfine field distribution and a correlated quadrupole interaction distribution as discussed in the text.

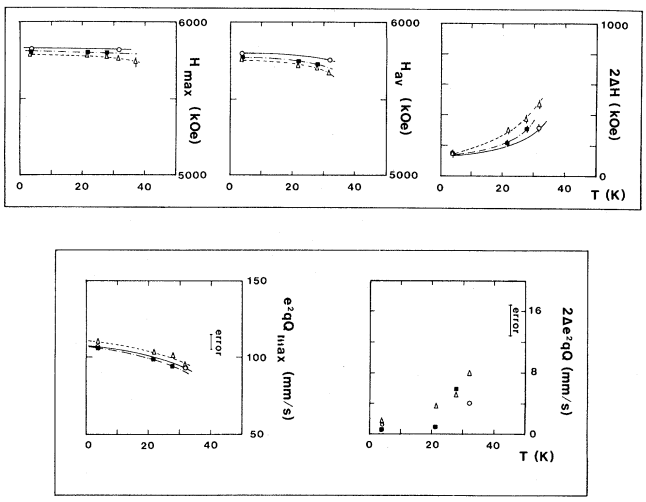

FIG. 6. Summary of the characteristic parameters of the hyperfine field distribution (top) and of the quadrupole interaction distribution (bottom) in ○, $Dy_{80}Au_{20}$; ■, $Dy_{80}Ga_{20}$; △, $Dy_{65}Al_{35}$. H_{max}, H_{av}, and $2\Delta H$ represent, respectively, the maximum H value, the average hyperfine field, and the width at half maximum of the skewed hyperfine field distribution. e^2qQ_{max} and $2\Delta e^2qQ$ are the maximum value and the width of the quadrupole interaction distribution, respectively.

V. DISCUSSION OF THE ^{161}Dy HYPERFINE RESULTS

A. Theoretical survey: Electronic Hamiltonian

Accepting the electronic Hamiltonian truncated to the quadratic CEF terms [Eq. (1)] one is able to calculate the electronic wave functions (Γ_i) and energy levels (E_i) arising from the crystal-field and exchange splitting of the ground J multiplet of the Dy^{3+} ion ($^6H_{15/2}$). The knowledge of the electronic structure in turn allows the calculation of the hyperfine parameters within established approximations.[15]

A major step in comparison to earlier works in rare-earth amorphous materials is provided by the present knowledge of the distribution of the quadratic CEF parameters since these are directly related to the lattice EFG components (q_z^{lat},η^{lat}) (Ref. 15) which have been measured in the corresponding europium and gadolinium alloys:[2,9]

$$B_2^0 = Kq_z^{lat}, \quad B_2^2 = B_2^0\eta^{lat} \tag{2}$$

with K estimated to $(3.3\pm0.5)\times10^{-18}$ K cm^2 V^{-1}.[16]

Also, the average modulus of the molecular field is known from the magnetic ordering temperature (T_f):

$$||H_{mol}|| = 3k_BT_f/g_J\mu_B(J+1)\ . \tag{3}$$

Hence, knowing all the parameters of the electronic Hamiltonian [Eq. (1)], the electronic structure is computed numerically. Calculations are performed for different orientations between the CEF and H_{mol} axes as a function of the quadratic CEF parameters.[17,18] The local moment orientation is deduced from energetical consideration as corresponding to the direction providing the maximum modulus of the magnetic moment.

B. The hyperfine interactions at ^{161}Dy

The hyperfine field H acting at the Dy nucleus is a sum of four contributions,

$$H = H_{4f}+H_{CP}+H_{OP}+H_N = H^{ion}+H_N\ , \tag{4}$$

corresponding respectively to the summed orbital and spin-dipolar fields created by the $4f$ open shell (H_{4f}), the core polarization of the inner electronic shells by the $4f$ moment (H_{CP}), the polarization of the $5d$-$6s$ conduction electrons by the $4f$ moment (H_{OP}), and the field

TABLE II. Summary of ^{161}Dy hyperfine results in amorphous $Dy_{1-x}X_x$ alloys below T_f. δ_{IS} is the isomer shift measured against the (Gd,Dy)F_3 source. W is the full width at half maximum (FWHM) of the Mössbauer resonance components. ΔH is the step of the cubic polynomial distribution function (i.e., the FWHM of the H distribution is $2\Delta H$).

	$Dy_{80}Au_{20}$		$Dy_{80}Ga_{20}$			$Dy_{65}Al_{35}$	
δ_{IS} (mm/s)	2.6±0.2		2.4±0.2			2.3±0.2	
W (mm/s)	5±1		5±1			5±1	
	T=4.2 K	T=32 K	T=4.2 K	T=28 K	T=4.2 K	T=28 K	T=32 K
H_{max} (kOe)	5830±50	5820±50	5800±50	5800±50	5790±50	5790±50	5780±30
ΔH (kOe)	70±10	160±20	70±10	180±20	70±20	120±30	230±30
e^2qQ_{max} (mm/s)	107±5	95±5	107±5	95±5	110±5	100±5	95±5
$e^2q_z^{lat}Q$ (mm/s)[a]	+28		+17 and −17			+19 and −19	
B_2^0 (K)[b]	+3.4		+2.1 and −2.1			+2.3 and −2.3	

[a]Principal component of the lattice EFG at Dy^{3+} calculated from e^2q_zQ at RE S-state ions in the corresponding $R_{1-x}X_x$ amorphous alloys (R=Gd^{3+} or Eu^{2+}) (Refs. 2 and 9).
[b]Calculated from $e^2q_z^{lat}Q$ at Dy^{3+} [Eq. (2)].

transferred from neighboring atoms via conduction electrons (H_N).[19]

H^{ion} is proportional to the thermal average of the local total angular momentum $\langle J_Z \rangle$. H_N corresponds to a thermal and spatial average: $H_N \propto (g_J-1)\langle\langle J_Z \rangle\rangle$. Thus, in an asperomagnetic amorphous alloy, H_N is predicted to be distributed both in magnitude and in direction. This term is argued to be negligibly small in comparison to H^{ion} by reference both to estimates in corresponding Eu and Gd alloys and to transferred field measurements at the ^{197}Au nucleus H_N(Au). Indeed, $|H_N|$ was smaller than 100 kOe at ^{151}Eu and 170 kOe at ^{155}Gd in ferromagnetic $R_{1-x}X_x$.[2,20] Scaling for the $(g_J-1)J$ factors and considering the asperomagnetic structure, an average value of the transferred field in the dysprosium alloy is calculated as $|H_N(\mathrm{Dy})| = \frac{1}{2}\cdot\frac{5}{7}|H_N(\mathrm{Gd})| \simeq 60$ kOe. This result is consistent with the measurements of transferred field at ^{197}Au which provide, respectively, 275 kOe in $Dy_{80}Au_{20}$ and 800 kOe in $Gd_{80}Au_{20}$ or $Eu_{80}Au_{20}$.

Hence, H reduces here to H^{ion} within reasonable approximation. By reference to metallic Dy compounds, the value of H^{ion} is evaluated for a pure $J_Z=\frac{15}{2}$ state (including H_{CP} and H_{OP}) to $H^{ion}(J_Z=\frac{15}{2})=H^{15/2}=5800\pm100$ kOe.[19] In the general case of electronic wave-function mixing, H^{ion} is evaluated for a level (Γ_i) as

$$H \simeq H^{ion}(\Gamma_i)=\langle \Gamma_i | \hat{J}_Z | \Gamma_i \rangle H^{15/2}/(\tfrac{15}{2}) , \quad (5)$$

where $\hat{J}_Z$ is the angular momentum operator. When several crystal-field levels are thermally populated at the temperature T, $H^{ion}(T)$ is calculated as an average over the contributions from each level at energy E_i:

$$H^{ion}(T)=\sum_i H^{ion}(\Gamma_i)e^{-E_i/k_BT} \Big/ \sum_i e^{-E_i/k_BT} , \quad (6)$$

and k_B is the Boltzmann constant.

The electric field gradient at the Dy nucleus arises from the nonisotropic charge distribution of both the $4f$ electrons and the neighboring ionic charges building up the solid. The lattice contribution is known from EFG measurements at S-state ions in the corresponding Eu or Gd alloys.[9] The deduced average lattice quadrupole coupling constants which are calculated by scaling for the respective nuclear moments are included in Table II. The distribution in sign for the principal component and in magnitude for η^{lat} are taken identical to those measured in the Eu alloys since the structural short-range order is independent of the RE element.[2,9]

The components of the EFG tensor produced by the $4f$ electrons are calculated as a Boltzmann average [similar to Eq. (6)] over the contributions from the populated levels (Γ_i):

$$e^2Qq_Z^{ion}(\Gamma_i)=\langle \Gamma_i | 3\hat{J}_Z^2-\hat{J}^2 | \Gamma_i \rangle e^2Qq_Z^{15/2}/105 ,$$
$$\eta^{ion}(\Gamma_i)=3\langle \Gamma_i | \hat{J}_+^2+\hat{J}_-^2 | \Gamma_i \rangle /2\langle \Gamma_i | 3\hat{J}_Z^2-\hat{J}^2 | \Gamma_i \rangle , \quad (7)$$

where $e^2Qq_Z^{15/2}$ is the quadrupole coupling constant corresponding to a pure $|J_Z=\frac{15}{2}\rangle$ state, i.e., 140±10 mm/s.[16]

It should be noticed that the principal systems of axes for the lattice and $4f$ EFG tensors will not coincide in general, particularly for an amorphous solid. In the following analysis, the asymmetry parameter of the total EFG tensor, which cannot be measured from magnetic ^{161}Dy Mössbauer spectroscopy, is neglected. This is consistent with the calculation of a negligibly small η^{ion} over the whole range of B_2^2 values (see below). The total asymmetry parameter (summed lattice and $4f$ terms), which depends on the relative orientations of the respective tensor principal axes, is calculated to be always inferior to 0.2 (Fig. 8). Hence, the lattice EFG contribution is treated as a perturbation of the $4f$ term and projected along the axial $4f$ component eq_Z^{ion}:

$$e^2Qq_Z=e^2Q[q_Z^{ion}+\tfrac{1}{2}q_z^{lat}(3\cos^2\theta-1+\eta^{lat}\sin^2\theta\cos2\varphi)] , \quad (8)$$

where θ and φ represent the polar angles defining the orientation of the lattice EFG principal axes with respect to the angular momentum $\vec{J}_Z$.

C. Computed distributions of the hyperfine parameters and comparison to experiment

The electronic configuration and the hyperfine parameters are computed with the experimental "quadratic" CEF

parameters (Table II) and with $||H_{mol}||=160$ kOe. Over the whole range of negative B_2^0, almost independent of the value of B_2^2, a well-isolated ground state of nearly pure $|J_Z=\frac{15}{2}\rangle$ nature is calculated; in this range of CEF parameters, corresponding to an easy-axis situation along the CEF principal axis ($\theta=0$), the first excited CEF level lies at approximately 110 K over the whole range of $\eta^{lat}=|B_2^2/B_2^0|$ values from zero to unity.

On the other hand, for the range of positive B_2^0, the local easy axis is perpendicular to the principal CEF axis ($\theta=\pi/2$) (easy-plane-like situation). Significant mixing of $|J_Z\rangle$ states is predicted for the range of positive B_2^0, particularly for small values of B_2^2 (i.e., small values of η^{lat}). Moreover, the first excited CEF level is between 40 K (for $\eta^{lat}=|B_2^2/B_2^0|=0$) and 110 K (for $\eta^{lat}=1$). It follows that in the ground-state level the total angular momentum J_z (i.e., H^{ion} or the local magnetic moment $\mu=g_J\mu_B\langle J_Z\rangle$) is significantly reduced in comparison to the free-ion value for positive B_2^0 and small value of B_2^2 (or η^{lat}) (Fig. 7); elsewhere, it is nearly constant and only slightly reduced in comparison to the free-ion value. One should notice that the J_Z reduction for positive B_2^0 and small B_2^2 increases significantly with temperature, via thermal population of the first excited level which is also lowest for this specific regime of the CEF parameters.

Similarly, the $4f$ contribution to the EFG in the ground-state level is reduced with respect to $q_Z^{15/2}$ over the whole range of B_2^2 values, especially in case of an easy-plane situation ($B_2^2=0$, $B_2^0>0$) (Fig. 8). However, because of the different orientations between q_z^{lat} and $\vec{J}$ according to the sign of B_2^0, the spread of the total EFG values is reduced in comparison to the one calculated for q_Z^{ion} alone (Fig. 8). Again, the relative reduction increases significantly with temperature, mostly in the regime of the easy-plane situation ($B_2^0>0$, $B_2^2\simeq 0$). The asymmetry parameter of the $4f$ EFG tensor, η^{ion}, is calculated as being negligibly small ($\lesssim 4\%$), consistent with the observation of the nearly-free-ion moment along the calculation (Z) direction. It is also of interest to notice the small sensitivity of the above features on the value of H_{mol} since comparable results are found for a range of H_{mol} values comprised between 100 and 200 kOe. Therefore, the probable distribution of this parameter, as well as its temperature dependence far from T_f, we have little effect on the local ionic properties.

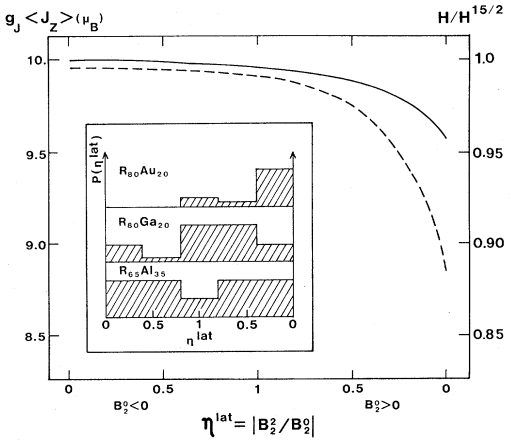

FIG. 7. Calculated Dy magnetic moment ($g_J\langle J_Z\rangle$) and reduced hyperfine field ($H/H^{15/2}$) represented as a function of $\eta^{lat}=|B_2^2/B_2^0|$ for $B_2^0=\pm 2.3$ K and $||H_{mol}||=160$ kOe. The heavy and dotted lines correspond to temperatures T of 0 and 28 K, respectively. The marginal distributions of η^{lat} deduced for the several $R_{1-x}X_x$ alloys from the lattice EFG measurements in the corresponding Eu and Gd alloys (Refs. 2 and 9) are represented as histogram plots.

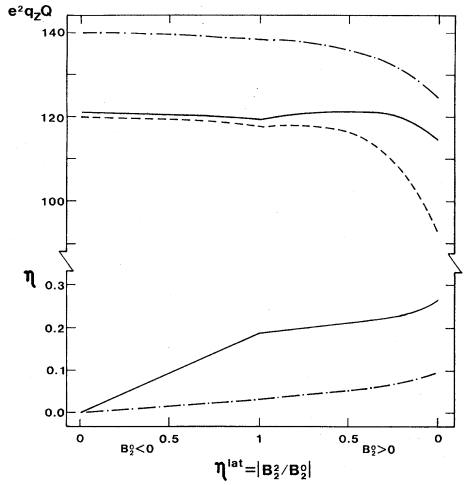

FIG. 8. Quadrupole coupling constant, e^2q_ZQ, calculated as a function of $\eta^{lat}=|B_2^2/B_2^0|$ for $B_2^0=\pm 2.3$ K and $||H_{mol}||=160$ kOe. Upper part, chained curve: ionic contribution $e^2Qq_Z^{ion}$ at $T=0$ K; heavy and dotted lines: summed ionic and lattice contribution e^2Qq_Z at $T=0$ and 28 K, respectively. Lower part, chained curve: η^{ion} alone at $T=0$ K; heavy line: upper limit of the summed ionic and lattice contribution to η at $T=0$ K.

With the knowledge of the distribution in sign of B_2^0 and in magnitude of the nonaxial B_2^2 term [Eq. (2)] one is able to compute the distribution of the hyperfine parameters for the several alloys under consideration. Amorphous $Dy_{65}Al_{35}$ represents an example of broadly distributed EFG parameters, with B_2^0 presenting approximately equal positive and negative sign probabilities and $|B_2^2/B_2^0|$ being distributed from zero to unity. The computations predict a skewed distribution for the hyperfine field, with a distribution width increasing significantly with temperature. Very satisfactory agreement is observed between experiment and calculation (Fig. 9).

The average quadrupole coupling constant is predicted to be significantly reduced with respect to the free-ion value, and to decrease with temperature, in agreement with experiment. However, ^{161}Dy experimental resolution does not allow an experimental examination of the predicted EFG distributions. Furthermore, the calculations predict a correlation between the distributions of the two parameters H and eq_Z. This cannot be reasonably ascertained from the data analysis; it also invalidates an attempt of further analysis assuming uncorrelated distribution of the quadrupole interaction.

On the other hand, amorphous $Dy_{80}Au_{20}$ represents a situation of more axial structural short-range order, with

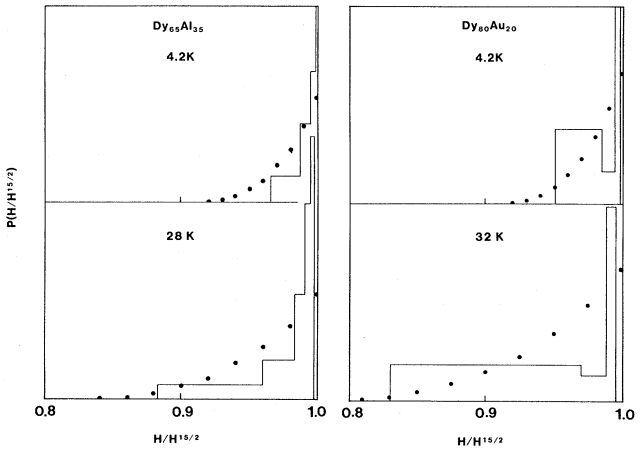

FIG. 9. Calculated (histogram) and measured (dots) distributions for the reduced hyperfine field ($H/H^{15/2}$) at $T=4.2$ and 32 K in $Dy_{65}Al_{35}$ and in $Dy_{80}Au_{20}$.

B_2^0 strongly weighted to positive values.[9] In comparison to $Dy_{65}Al_{35}$ the computations predict a larger distribution width and a larger temperature dependence for both the hyperfine field and quadrupole interaction (Figs. 7 and 8); however, this feature is determined by the precise extent of the η distribution close to zero value, which is uncertain. Furthermore, the predicted changes are small in comparison to the precision of the data analysis and cannot be established safely from experiment (Fig. 9).

The magnetization curves agree qualitatively with the predictions from the RMA model, although precise analysis is impossible in the range of available external fields. The slightly increased remanent magnetization observed at 4.2 K for $Dy_{80}Au_{20}$ in comparison to the other two alloys (Fig. 3) is tentatively assigned to the larger probability for an easy-plane situation,[21] in agreement with the calculations. In $Dy_{80}Au_{20}$, this implies a locally nonisotropic distribution of the Z axes, i.e., a departure from the ideal asperomagnetic structure, which will allow an enhanced fraction of Dy moments to be oriented in their easy plane by ferromagnetic interaction.

The analysis of the distributions of the hyperfine parameters has concentrated earlier on the quadrupole interaction, under the assumption of negligible or symmetrical hyperfine field distribution.[8,22] Such a procedure is found unacceptable both from a spectroscopical point of view, since significant improvement of the fits is provided when including an asymmetrical hyperfine field distribution, and from a physical point of view, when considering the distributions predicted from the quadratic CEF parameters. Hence, the former claim for the experimental demonstration of the uniaxial RMA on the basis of the small distribution of the quadrupole coupling constant,[1,8] i.e., a strict angular correlation between q_Z^{ion} and q_z^{lat} is invalidated from the present analysis and calculations. Actually, our theory predicts that the moment is parallel to the CEF principal axes for $B_2^0<0$ and perpendicular for $B_2^0>0$, but this difference cannot be detected from Mössbauer-spectroscopy measurement by lack of spectral sensitivity.

VI. SUMMARY AND CONCLUSIONS

^{161}Dy Mössbauer spectroscopy and bulk magnetic properties are combined in order to elucidate the crystalline electric field effects in a series of amorphous dysprosium alloys. A detailed reconsideration of the ^{161}Dy hyperfine results points to a skewed shape of the distribution of hyperfine field whereas the precision of the analysis of the quadrupole parameters is limited by the spectroscopic resolution. Using the lattice component to the EFG collected previously at S-state (Eu^{2+}, Gd^{3+}) ions, a theoretical analysis of the measured distributions of hyperfine parameters is performed. Within precision limits, the experimental results are reproduced by a theoretical model including the distributions of the quadratic CEF parameters (B_2^0 and B_2^2) which are known from the lattice EFG results. It should be pointed out that the uniaxial RMA model is certainly insufficient to reproduce the hyperfine results; actually, this simplified approximation is already ruled out from the lattice EFG results alone, which directly point out to the existence of the nonaxial quadratic CEF term (B_2^2).

The widely different distributions of the CEF parameters in the considered series of compounds (corresponding to a highly disordered structure in $Dy_{65}Al_{35}$ and a nearly axial symmetry in $Dy_{80}Au_{20}$) turn out to be barely reflected from the hyerfine data. However, this behavior fully fits with the theoretical calculations since little difference is predicted for the respective situations for a dysprosium alloy. On the other hand, calculations predict a more sensitive dependence on the type of considered structural short-range orders whenever the Stevens coefficient α_J would be positive, e.g., in Er^{3+} or Tm^{3+} alloys.

[1]R. W. Cochrane, R. Harris, and M. J. Zuckermann, Phys. Rep. **48**, 1 (1978).
[2]J. M. Friedt, M. Maurer, J. P. Sanchez, and J. Durand, J. Phys. F **12**, 821 (1982).
[3]R. Asomoza, I. A. Campbell, A. Fert, A. Lienard, and J. P. Rebouillat, J. Phys. F **9**, 349 (1979).
[4]J. M. D. Coey, T. R. McGuire, and B. Tissier, Phys. Rev. B **24**, 1261 (1981).
[5]S. von Molnar, T. R. McGuire, and R. J. Gambino, J. Appl. Phys. **53**, 7666 (1982).
[6]A. Fert and I. A. Campbell, J. Phys. F **8**, L57 (1978).
[7]E. Borchi and S. de Gennaro, J. Phys. F **11**, L47 (1981).
[8]J. M. D. Coey, J. Chappert, J. P. Rebouillat, and T. S. Wang, Phys. Rev. Lett. **36**, 1061 (1976).
[9]M. Maurer, J. M. Friedt, and G. Krill, J. Phys. Met. Phys. **13**, 2389 (1983).
[10]S. J. Poon and J. Durand, Phys. Rev. B **16**, 316 (1977).
[11]K. H. J. Buschow and N. M. Beekmans, in Proceedings of 3rd Rapidly Quenched Metals, Brighton, 1978, edited by B. Cantor [Met. Soc. London **2**, 133 (1978)].
[12]B. Boucher, A. Lienard, J. P. Rebouillat, and J. Schweitzer, J. Phys. F **9**, 1421 (1979).
[13]J. J. Rhyne, in *Handbook of Physics and Chemistry of Rare Earths*, edited by K. A. Gschneider and L. R. Eyring (North-

Holland, Amsterdam, 1979), Vol. II, p. 259 (1979); P. d'Antonio, J. Konnert, J. J. Rhyne, and C. R. Hubbard, J. Appl. Cryst. **15**, 452 (1982).

[14]M. Maurer and J. M. Friedt (unpublished).

[15]R. G. Barnes, R. L. Mössbauer, E. Kankeleit, and J. M. Poindexter, Phys. Rev. **136**, A 175 (1964).

[16]J. M. Friedt, G. K. Shenoy, and B. D. Dunlap, J. Phys. (Paris) Colloq. **40**, C2-243 (1979).

[17]B. D Dunlap, G. K. Shenoy, J. M. Friedt, M. Meyer, and G. J. McCarthy, Phys. Rev. B **18**, 1936 (1978).

[18]O. Danielsen and P. A. Lindgard, Danish Atomic Energy Commission—Research Establishment Risö Report No. 259, 1972 (unpublished).

[19]See, e.g., B. Bleaney, in *Magnetic Properties of Rare Earth Metals,* edited by R. J. Elliott (Plenum, London, 1972), p. 383; G. J. Bowden, R. K. Day, and P. Martinson, J. Phys. F **8**, 2051 (1978).

[20]M. Maurer and J. M. Friedt, J. Phys. F **13**, 2175 (1983).

[21]E. Callen, Y. J. Liu, and J. R. Cullen, Phys. Rev. B **16**, 263 (1977).

[22]J. P. Sanchez, M. Maurer, and J. M. Friedt, Proceedings of the International Conference on the Applications of the Mössbauer Effect, 1981, Jaipur [Proc. Ind. Nat. Sci. Acad. (Spec. Issue) 353 (1982)].